RSC Advances

ROYAL SOCIETY OF CHEMISTRY

www.rsc.org/advances

Content entry

A robust superhydrophobic surface with excellent mechanical abrasion and corrosion resistance, self-cleaning ability as well as long-term stability is fabricated by a novel anodic oxidation and self-assembly process.

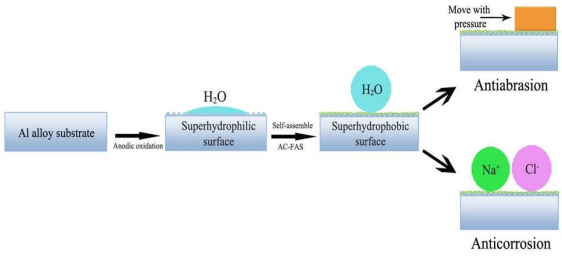

Facile Fabrication of a Robust and Corrosion Resistant Superhydrophobic Aluminum Alloy Surface by a Novel Method

Cansen Liu, *Fenghua Su*[*], *Jizhao Liang*
School of Mechanical and Automotive Engineering, South China University of Technology, Guangzhou 510640, China

Abstract: This work reports a novel method including anodic oxidation and self-assembly process for controllable fabrication of a robust superhydrophobic Aluminum (Al) alloy surface. The superhydrophobic surface with a water contact angle of 157.5± 0.5° and a sliding angle of 3 ± 0.7° derives from its hierarchical micro-nanostructure and the assembly of low surface energy fluorinated components on it. Furthermore, the transformation from superhydrophilicity to superhydrophobicity can be achieved by adjusting the modification process for the constructed surface. The anti-scratch tests show that the superhydrophobic surface has good mechanical stability. It maintains superhydrophobicity after mechanical abrasion against P400 grit SiC sandpaper for 0.4 m and P800 grit sandpaper for 0.8 m, respectively, at the applied pressure of 3.60 kPa. The potentiodynamic polarization and electrochemical impedance spectroscopy tests show that the as-prepared superhydrophobic surface has excellent corrosion resistance. In addition, the as-prepared superhydrophobic surface has self-cleaning ability and good long-term stability. It is believed that the facile fabrication process offer an effective and promising applications for fabricating a robust, anticorrosion and large scale superhydrophobic Al alloy surface.

Keywords: Superhydrophobic surface; Mechanical stability; Anticorrosion; Self-cleaning; Aluminum alloy

[*] Corresponding author. Tel./fax: +86 20 87112341
E-mail address: fhsu@scut.edu.cn

1. Introduction

In recent years, the fabrication of superhydrophobic surfaces with a water contact angle (CA) larger than 150° and a water sliding angle (SA) less than 10° has attracted tremendous interest for researchers around the world for its great importance in fundamental research as well as its widespread potential applications in various industrial fields[1, 2]. Superhydrophobic surfaces have many practical applications in various areas, such as self-cleaning[3], anti-icing[4], oil-water separation[5], antibacterial adhesion[6] and anticorrosion[7, 8]. It is reported that superhydrophobic surfaces can be fabricated by either coating a special micro-nanostructures surface with low surface energy stuffs or constructing a proper roughness on a hydrophobic surface[9-12]. Up to now, a great number of methods have successfully developed to fabricate artificial superhydrophobic surfaces, such as plasma treatment[13], sol gel[14], chemical vapor deposition[15], chemical etching[16], electrospinning[17], solution-immersion[18], colloidal template[19], laser fabrication[20] and electrodeposition[21, 22].

Although different artificial superhydrophobic surfaces have been fabricated by various methods, few products were practical application in industrial because of their poor mechanical abrasion resistance, instability to finger contact, surface chemical instability and short-term stability. Improving the mechanical stability and chemical stability of superhydrophobic surfaces become the urgent demand for their practical applications[23]. Zhu et al.[24, 25] evaluated the mechanical stability of the constructed superhydrophobic metal/polymer composite and fabric surfaces by a simple finger pressing and scratch test. She et al.[26] evaluated the mechanical stability and chemical stability of the as-prepared

superhydrophobic surface constructed on magnesium alloy substrate. They found the surface still maintained superhydrophobicity after sliding against P800 grit SiC sandpaper for 0.7 m under a pressure of 1.2 kPa. In addition, this superhydrophobic surface also displays good chemical-stability as functions of the ionic strength and pH value. In our previous work[27], a superhydrophobic nickel deposit was fabricated on the Cu substrate. The superhydrophobic deposit exhibits excellent mechanical abrasion and corrosion resistance. It maintains superhydrophobicity after mechanical abrasion against P800 grit SiC sandpaper for 1.0 m at the applied pressure of 4.80 kPa.

Aluminum (Al) and its alloys are widely used in various industrial fields because they possess much predominance performance, such as high-specific strength, excellent heat, electrical conductivities and low-specific weight[28, 29]. The anodic oxidation of Al materials has clearly gained enormous importance both from a scientific point of view and for technology and industrial production[30]. However, the application of the anodic oxidation technology is limited in marine environment because the porous oxide surface is easily to be eroded by Cl^{-1} in seawater[31]. A few reports proved that superhydrophobic surfaces were effective in preventing Al alloy corrosion[32-34] . He et al.[32] found the super-hydrophobic surface significantly improved the corrosion resistance of Al in sterile seawater. Feng et al.[33] found that the superhydrophobic Al alloy has the better corrosion resistance than bare Al alloys. Unfortunately, the mechanical and chemical stability of the fabricated superhydrophobic Al alloy surfaces were not paid much attention in these literatures.

In this work, a facile and low-cost method is used to produce superhydrophobic Al alloy surfaces. The fabrication process consists of two steps. Firstly, the rough surface with

hierarchical micro-nanostructure is fabricated on the Al alloy surface using anodic oxidation process. Secondly, the modified surface was assembled with a fluorinated components film by a simple process. The as-prepared surface displays superhydrophobicity with a water contact angle of 157.5± 0.5° and a sliding angle of 3 ± 0.7°. Additionally, the superhydrophobic surface shows excellent mechanical stability and corrosion resistance, self-cleaning ability as well as long-term stability.

2. Experimental section

2.1 Materials

Commercially available aluminum alloy sheets were provided by Guangzhou Meicai non-ferrous metal material trade Co. Ltd., China. Analytical grade Sodium chloride (NaCl) was obtained from Taishan Yueqiao Reagent Plastic Co. Ltd., China. (Heptadecafluoro-1, 1, 2, 2-tetradecyl) triethoxysilane ($CF_3(CF_2)_7(CH_2)_2Si(OC_2H_5)_3$, AC-FAS) was supplied Guangzhou Liyuan Chemical Meterial Company, China. Anhydrous ethanol was provided by Guangzhou Donghong Chemical Plant, China. All chemical reagents are analytical and used without purification.

2.2 Sample preparation

An Al alloy plate with a size of 40× 20 ×2 mm was used as the anode for anodic oxidation in 0.2 M NaCl electrolyte. Another Al alloy plate with the same size was used as the cathode. Prior to anodizing, the plate surfaces were polished mechanically using abrasive P600 and P800 grit SiC sandpapers and sequentially cleaned ultrasonically with distilled water and acetone to remove contamination on the substrate surface. The anodic oxidation

was conducted using a current density of 400 mA cm^{-2} for different time and the distance between two electrodes was fixed at 10 mm. After anodic oxidation, the anodic Al alloy plate was rinsed with distilled water and dried for subsequent modification. The bare Al alloy surface and the anodic Al alloy surface were dubbed as Surface-I and Surface-III, respectively.

In the next modification, the anodized Al alloy was immersed in a 5.0 wt % AC-FAS ethanol solution for 1min and subsequently heated at 100℃ for 10 min in an oven to obtain the superhydrophobic surface. The superhydrophobic surfaces were dubbed as Surface-IV_X (x: the anodic oxidation time in the first step). For comparison, the bare Al alloy was also treated with the same immersing and heating process and the modified surface was dubbed as Surface-II.

2.3 Characterizations

The water contact angles and sliding angles were measured with approximately 5 μL water droplet using a measuring apparatus (Dataphysics OCA40 Micro) at ambient temperature. The values reported are the average of five measurements made on different positions of the sample surface. Surface morphologies of various samples were studied using a field emission scanning electron microscope (FESEM, Nova NanoSEM 430). The chemical compositions of the samples were investigated with a Fourier-transform infrared spectrophotometer (FTIR, Bruker Vector 33) and X-ray photoelectron spectrometer (XPS, Kratos Axis Ultra DLD). The sample surface roughness was characterized with a BMT Expert 3D surface profile measurement system. The mechanical stability of the obtained samples was evaluated by scratch test. The scratch test was carried out on a homemade

scratch tester with different grit size SiC sandpapers as abrasion surface. The sample surfaces were tested facing these abrasion surfaces with varying distance.

Electrochemical corrosion test was carried out in a three electrode cell. A platinum plate and saturated silver/silver chloride (Ag/AgCl) electrode were used as the counter and reference electrode, respectively. The fabricated superhydrophobic surface or the bare Al surface was used as the working electrode. Measurements were performed by an electrochemical workstation (CorrTest CS310, Wuhan Corr Test Instrument Co. Ltd., China) at room temperature with neutral 3.5 wt. % NaCl solution as corrosive medium. Before electrochemical tests, samples were mounted using paraffin wax with surface area of 1 cm^2 exposed to the corrosive medium. All the samples were immersed for 30 min, allowing the system to be stabilized before the potentiodynamic polarization and electrochemical impedance spectroscopy (EIS) tests. The potentiodynamic polarization curves were recorded at a sweep rate of 0.5 mV s^{-1} from −200 to 200 mV versus the open circuit potential. As to EIS measurements, the employed amplitude of the sinusoidal signal was 10 mV, and the frequency range studied was from 10^5 to 10^{-2} Hz. The average value from four replicates for each kind of specimen was reported.

3. Results and discussion

3.1 Wettability, morphology and chemical compositions

Fig. 1 shows the images of the water contact angles on different Al alloy surfaces. It is clear that the surface wettability of these samples is affected by the modified methods. As shown in Fig. 1a, the untreated Al alloy substrate (Surface-I) is hydrophilicity with contact angle

approximately 97.9°. After modified with AC-FAS but without anodic oxidation process, the modified surface (Surface-II) is also hydrophilicity because of its contact angle around 114.7° (Fig. 1b). Interestingly, the water droplet completely spread on the Al surface (Surface-III) that is only modified with anodic oxidation prior to AC-FAS modification, as shown in Fig. 1c. The contact angle around 0^o suggests the anodized Al alloy surface is superhydrophilic. It is because the volume of the hydrophilic alumina and the roughness (Table 1) of this surface are extremely increased after the anodizing process [35]. However, the anodized Al alloy surface transforms from superhydrophilicity to superhydrophobicity with a contact angle of 157.5^o after modification with AC-FAS. It is clear that both anodic oxidation and AC-FAS modification are necessary for fabricating superhydrophobic Al alloy surface.

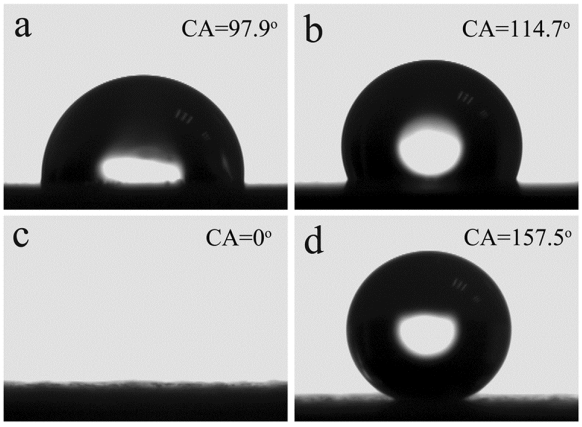

Fig. 1 Images of water droplets on various surface (insert: the contact angle value of the water droplet) (a: Surface-I; b: Surface-II; c: Surface-III; d: Surface-IV_9)

Influence of anodic oxidation time on the contact angles and sliding angles of the as-prepared superhydrophobic surfaces is shown in Fig. 2. When the anodic oxidation was

conducted for 1 min, the contact angle rapidly increases to 151°, indicating that it is a rapid way to fabricate superhydrophobic surface. However, the water sliding angle on this surface cannot be tested because the water droplet adheres to the surface even if the surface was tilted to 180°. This result might be attributed to the weak etching to the Al alloy surface by only 1 min anodic oxidation. Table 1 shows the surface roughness of this surface is only increased to 2.92 μm from 0.76 μm of the bare Al alloy surface. The contact angle increases to 153° and the sliding angle decreases to 20° when the anodic oxidation time was increased to 3 min. As the processing time prolongs, the contact angle increases, accompanying with the decrease of the sliding angle. When the processing time was 9 min, the resulting superhydrophobic surface displays the biggest contact angle of 157.5° and the smallest sliding angle of 3°.

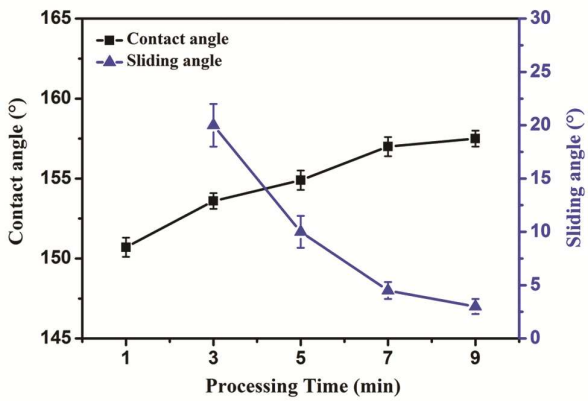

Fig. 2 Influence of anodic oxidation time on the contact angles and sliding angles of the superhydrophobic surfaces.

Fig. 3 shows the SEM images of various Al alloy surfaces. The bare Al alloy surface (Surface-I) is also shown as a reference (Fig. 3a). Fig. 3b shows that Surface-II is smoother

than the bare Al alloy surface, which derives from the coating of AC-FAS on the bare Al surface. The morphologies of the superhydrophobic surfaces (Surface-IV_X) are shown in Figs. 3c-l. As shown in Figs. 3c-e, the superhydrophobic surface anodized for 1 min (Surface-IV_1) is composed of many micro-pores and protuberances. However, some flat areas are observed on this surface, which confirms the weak etching to the bare Al surface by only 1 min anodic oxidation. As shown in Figs. 3f-k, the superhydrophobic surfaces become rougher and there are more micro-pores and protuberances observed with the increase of the anodic oxidation time. The protuberances and micro-pores are irregular and seem to form the coral network hierarchical structure. Figs. 3j and k show that the hierarchical structure looks like the accumulation of micro-nanometer empty boxes. This hierarchical micro-nanostructure might be related to the superhydrophobicity of the modified Al alloy surface (Surface-IV_9). Interestingly, Figs. 3l and 3j show that the superhydrophilic surface (Surface-III) has similar morphology with the superhydrophobic surface (Surface-IV_9), which indicates that the morphology is important but not the only factor to determine the superhydrophobicity of the surface. The mechanism to obtain the superhydrophobic Al alloy surface will be illustrated in the following sections.

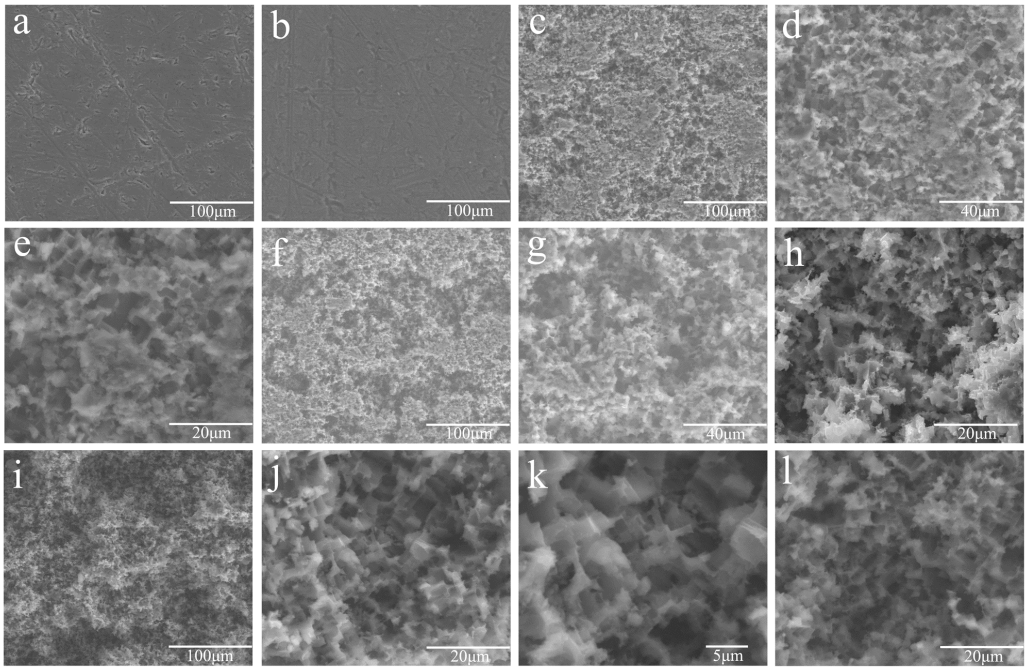

Fig. 3 SEM images of various Al alloy surfaces. (a: Surface-I; b: Surface-II; c-e: Surface-IV_1; f-h: Surface-IV_5; i- k:Surface-IV_9; l:Surface-III)

Surface roughness of various Al alloy surfaces is shown in Table 1. The bare Al alloy substrate (Surface-I) has a surface roughness around 0.76 μm. The surface modified with AC-FAS (Surface-II) shows the decreased surface roughness of 0.36 μm. The surface roughness of the superhydrophilic surface (Surface-III) and the superhydrophobic surfaces (Surface-IV_X) are much higher than the bare Al alloy substrate. The superhydrophilic surface displays the highest surface roughness of 11.86 μm. The superhydrophobic surface modified with 1 min anodic oxidation shows the surface roughness of 2.92 μm. It is rapidly increased to 6.38 μm and 11.64 μm after 5 and 9 min anodic oxidation, respectively. As is well known, the surface roughness must reach the Cassie-Baxter state[36] to obtain a superhydrophobic surface. But the surface roughness is by no means the only factor to

determine the superhydrophobicity of the surface. Although Surface-III and Surface-IV_9 almost have the same surface roughness (Table 1), Surface-IV_9 is superhydrophobicity that is contrary to the superhydrophilic Surface-III. The contact angle of Surface-IV_5 is only slightly increased to 155^o from 151^o of Surface-IV_1, even if its surface roughness is greatly increased to 6.38 μm from 2.92 μm. We believed that the chemical composition is another decisive factor to determine the wettability of the modified surface besides the morphology and surface roughness.

Table 1. Average surface roughness of various surfaces

Sample	Surface-I	Surface-II	Surface-III	Surface-IV_1	Surface-IV_5	Surface-IV_9
Roughness (μm)	0.76	0.36	11.86	2.92	6.38	11.64

FTIR spectrum of the superhydrophobic surface is shown in Fig. 4a. A broad absorption band at 1000-1130 cm^{-1} resulting from the asymmetric stretching of Si-O-Si is found for the superhydrophobic surface. Three absorption bands at around 1149, 1206 and 1240 cm^{-1} that are assigned to C-F stretching vibration of $–CF_3$ and $–CF_2$ groups from the AC-FAS molecules are observed on the superhydrophobic surface. These results confirm that AC-FAS molecules have been successfully self-assembled on the superhydrophobic surface. Fig. 4b displays the XPS spectra of the superhydrophobic surface. The superhydrophobic surface exhibits strong signals of F1s, C1s and O1s and weak signal of Si2p. Fig. 4c shows high-resolution of C1s. The C1s peaks located at 292.2eV and 290.0eV are assigned to the carbon atom of $–CF_3$ and $–CF_2$, respectively. The peak located at 283.8eV is assigned to the carbon atom of –C-C and –C-H. The peak at 282.2eV is attributed to the carbon atom of

–C-Si. These results further demonstrate that the AC-FAS molecules have successfully assembled on the superhydrophobic surface.

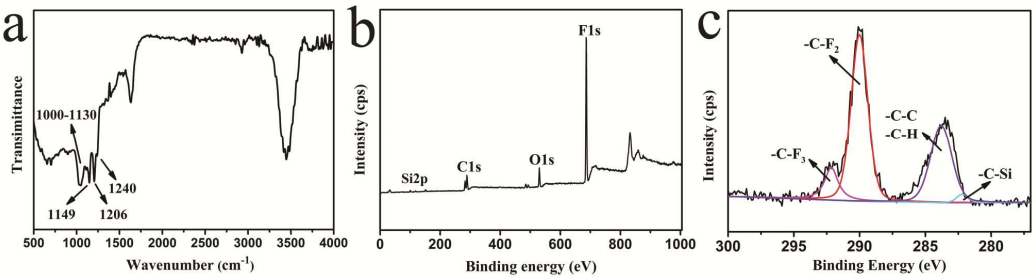

Fig. 4 a) FTIR spectrum of the superhydrophobic surface (Surface-IV_9); b) XPS survey spectra and c) High-resolution of C1s of this surface.

From the above analysis, it can be concluded that the superhydrophobic surface derives from its special micro-nanostructure and chemical compositions. The morphology evolution of the sample surface modified by the anodic oxidation and the self-assemble of AC-FAS can be displayed as Fig. 5a. A rough surface was firstly achieved on the Al alloy substrate by the anodic oxidation. The rough surface with hierarchical micro-nanostructures has been confirmed to favor the formation of the superhydrophobic surface[24, 37]. However, the rough surface is a necessary but not sufficient to achieve superhydrophobic surface. The surface wettability is also governed by its chemical compositions besides the surface morphology. The results of the FTIR and XPS measurements confirm that the AC-FAS have successfully self-assembled on the anodic Al alloy surface. Fig. 5b elaborates the formation mechanism of the self-assembled AC-FAS film on the rough Al alloy surface. The AC-FAS molecules react with the –OH groups of the anodized surface to form a self-assembled film on the surface with the help of heating. The assembled AC-FAS film

can reduce the free energy of the surface effectively because of its $–CF_3$ group with a surface energy of 6.7 mJ m^{-2} and $–CF_2$ group with a surface energy of 18 mJ m^{-2}. It can be concluded that the superhydrophobicity of the resulting surface derives from its rough surface with hierarchical micro-nanostructures and the presence of low-surface-energy fluorinated components on it.

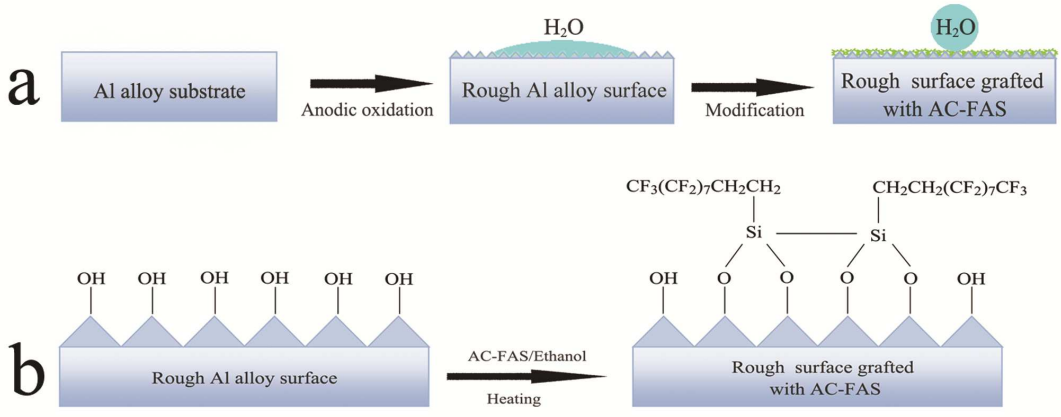

Fig. 5 a) Morphology evolution of the surface modified by anodic oxidation and then by AC-FAS modification; b) Formation mechanism of the self-assembled AC-FAS film on the anodic Al alloy surface.

3.2 Mechanical stability

Scratch tests were reported to be an effective method to evaluate the mechanical abrasion resistance of the superhydrophobic surfaces[26, 37]. In this work, the scratch tests were carried out using different grit size of SiC sandpapers as abrasion surface, as shown in Fig. 6a. The superhydrophobic surfaces facing the abrasion material were tested at a speed of 4-5 mm s^{-1} with varying sliding distance. Fig. 6b shows the variations of the contact angles with increasing abrasion distance for the superhydrophobic surface after mechanical abrasion against different grit size SiC sandpapers at the applied pressure of 3.6 kPa. It can be seen

that the contact angles decrease with the increase of abrasion distance, irrespectively of the grit size of the used SiC sandpaper. In addition, to maintain the superhydrophobicity (CA>150^{o}) for the modified surfaces, the abrasion distances are reduced with the increase of the grit size of the used SiC sandpapers. But in general, the modified Al surfaces can maintain superhydrophobicity after abrasion against P400 grit SiC sandpaper for 0.4 m and against P800 grit sandpaper for 0.8 m, respectively, at the applied pressure of 3.60 kPa. The results show that the as-prepared superhydrophobic surface has excellent mechanical abrasion resistance. It is much better than other reported superhydrophobic magnesium (Mg) alloy surface[26]. The superhydrophobic Mg Alloy surface cannot endure the abrasion distance over 0.7 m at the applied pressure of 1.2 kPa.

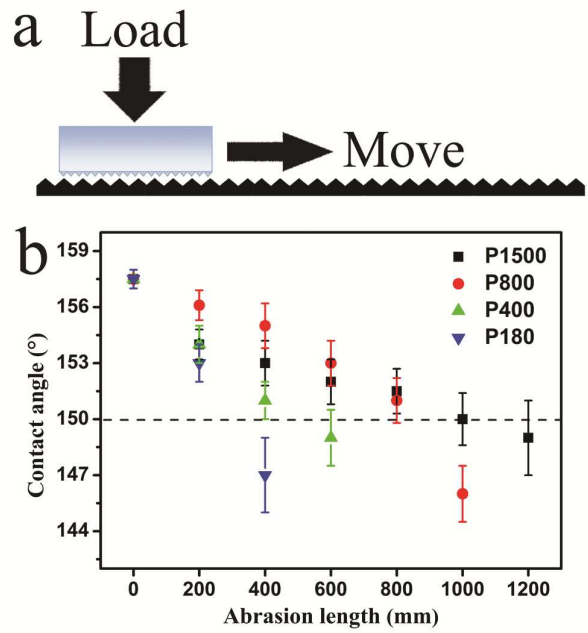

Fig. 6 a) Schematic illustration of the scratch test; b) Variations of the contact angles of the superhydrophobic surfaces after mechanical abrasion against different grit size SiC sandpapers at the applied pressure of 3.6 kPa

Fig. 7 displays the SEM images of the resulting superhydrophobic surfaces after abrasion against P800 grit SiC sandpaper for 0.2 m and 1.0 m at the pressure of 3.6 kPa. As shown in Figs. 7a and a-i, only a few scratches are observed on the superhydrophobic surface after abrasion for 0.2 m, which suggests that the surface is slightly scratched by the hard sandpaper. Therefore, the surface maintains superhydrophobicity (Fig. 6b). As the sliding distance increases to 1.0 m, the surface is featured with severe abrasion wear (Figs. 7b and b-i). The upper layer of the superhydrophobic surface was destroyed by mechanical abrasion resulting in the remove of the hierarchical micro-nanostructures in this layer. As a result, the contact angle of this surface is decreased to 146 ^{o} after abrasion for 1.0 m (Fig. 6b). Meanwhile, the superhydrophobic surface is rough with the surface roughness of 11.64 μm (Table 1). Although the hierarchical micro-nanostructures on the upper layer was destroyed by mechanical abrasion, some of these structures still exists in the rough surface (Figs. 7b and b-i). This might be the reason that the surface still has large contact angle of 146^{o} after severe abrasion for 1.0 m at the pressure of 3.6 kPa.

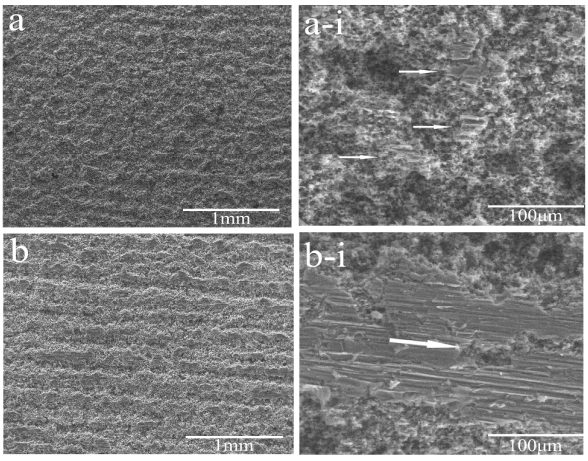

Fig. 7 SEM images of the superhydrophobic surface after abrasion against P800 grit SiC sandpaper for 0.2 m (a and a-i) and 1.0 m (b and b-i) at 3.6 kPa

3.3 Corrosion resistance

The potentiodynamic polarization curves of the bare Al alloy substrate and the superhydrophobic surface measured in 3.5 wt.% NaCl solution are shown in Fig. 8a. The corrosion potential (E_{corr}), corrosion current density (i_{corr}) and corrosion rate that are calculated using the program CorShow from the potentiodynamic polarization curves are listed in Table 2. The superhydrophobic surface displays much better corrosion resistance than the bare Al alloy substrate due to its more positive E_{corr}, lower i_{corr} and corrosion rate. The E_{corr} of the superhydrophobic surface is about 100 mV more positive than the bare Al alloy substrate. In addition, the i_{corr} of the superhydrophobic surface is approximately 2% that of the bare Al alloy substrate. The superhydrophobic surface exhibits very low corrosion rate, approximately 50 times decrease from the bare Al alloy substrate. It can be concluded that the as-prepared superhydrophobic surface has excellent corrosion resistance that can protect the bare Al alloy substrate from corrosion effectively.

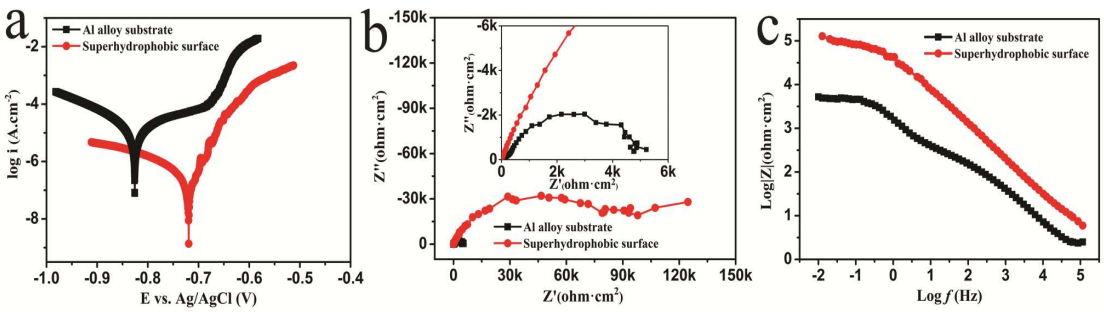

Fig. 8 Potentiodynamic polarization curves (a), Nyquist plots (b) and Bode plots (c) of the bare Al alloy substrate and the as-prepared superhydrophobic surface measured in 3.5 wt.% NaCl solution.

Table 2. Corrosion potential (E_{corr}), corrosion current density (i_{corr}) and corrosion rate of the Al alloy substrate and superhydrophobic surface

Sample	E_{corr} (mV)	i_{corr} (A·cm^{-2})	Corrosion rate(mm·a^{-1})
Al alloy substrate	-825.8	2.11×10^{-5}	2.29×10^{-1}
Superhydrophobic surface	-719.1	4.18×10^{-7}	4.55×10^{-3}

The Nyquist plots and Bode plots of the bare Al alloy and the superhydrophobic surface measured in 3.5 wt.% NaCl solution are shown in Figs. 8b and 8c, respectively. It is well know that the diameter of the capacitive loop in the Nyquist plots represents the polarization resistance of the work electrode. As shown in Fig. 8b, the superhydrophobic surface exhibits an impedance value around 2.0×10^5 Ω·cm^2 that is 35 times higher than the Al alloy substrate. It is clear that the superhydrophobic surface possesses a higher impedance modulus than the bare Al alloy substrate at low frequency, as shown in Fig. 8c. These results further confirm that the as-prepared superhydrophobic surface has better corrosion resistance than the bare Al alloy substrate.

Fig. 3 has showed that the superhydrophobic surfaces are featured with the hierarchical structure that is composed of the accumulation of micro-nanometer empty boxes. The air can be trapped in these micro-nanometer empty boxes according to the Cassie–Baxter equation[38, 39]. Therefore, the water drop from the corrosive solution might be suspended on the superhydrophobic surface. To confirm that, the as-prepared superhydrophobic surface was immersed in and then taken out from the 3.5 wt.% NaCl solution. The process is shown in Figs.9a-c. As shown in Fig. 9b, the superhydrophobic surface appears as a silver mirror when it is immersing in the solution. This mirror-like phenomenon is due to an air layer

between water and the superhydrophobic surface[40]. The superhydrophobic surface is completely dry after taking out from the solution (Fig. 9c), indicating that the surface is completely nonstick to the corrosive water. The result confirms that the air is indeed trapped in groove of surface and the liquid forming a convex surface between the interface of liquid and air for the capillary. The trapped air can prevent corrosive media from penetrating into the surface effectively and provides a good corrosion protection for the surface.

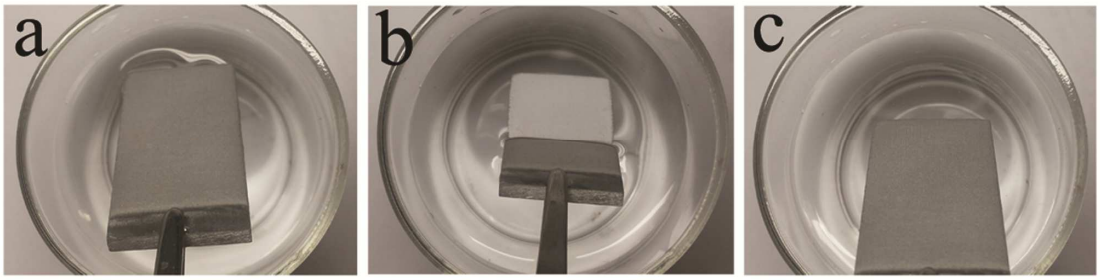

Fig. 9 (a-c) The process of the as-prepared superhydrophobic surface by immersing in and then taking out from the 3.5 wt.% NaCl solution. (Supporting Information Video 1: Air trapped test of the superhydrophobic surface by immersing in and then taking out from 3.5 wt.% NaCl solution.)

3.4 Self-cleaning effect

The self-cleaning effect of the as-prepared superhydrophobic surface is investigated by applying chalk dust as contaminants to the surface. Fig. 10 displays the evolution process of self-cleaning effect. The spherical water droplet began to roll quickly with removing the chalk dust, which might due to the result of joint action of high capillary forces induced by the water droplet and weak adhesion of the powder particle to the superhydrophobic surface.

It can be seen that the dusted sample become clean after washing by several droplets. The dusts in the experiments are far more than those in most natural environments, while the superhydrophobic surface shows the self-cleaning ability. It indicates that the superhydrophobic surface can protect substrates from pollution in practical applications.

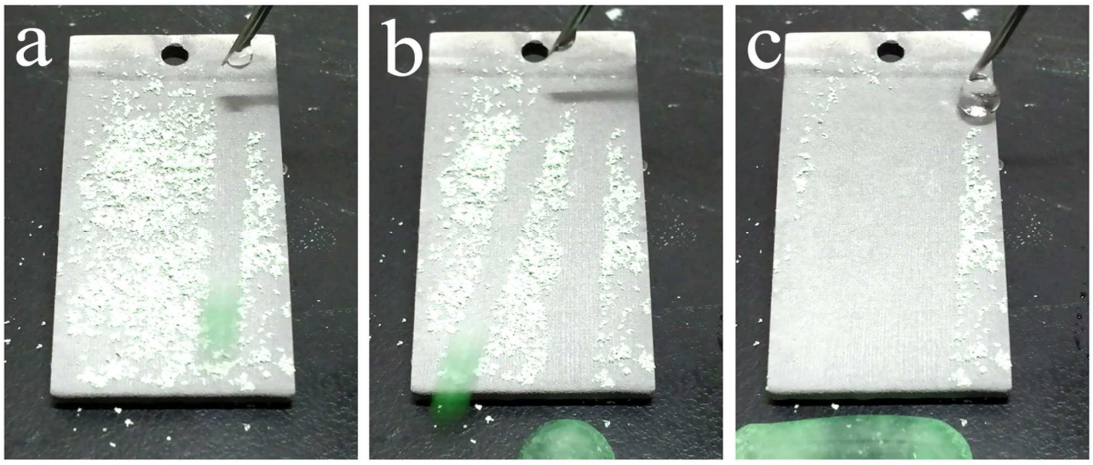

Fig. 10 (a-c) Evolution process of self-cleaning behavior of the superhydrophobic surface. (Supporting Information Video 2: Self-cleaning test of the superhydrophobic surface with chalk dust as contaminants)

3.5 Long-term stability

The long-term stability is very important to determine the feasibility of the superhydrophobic surface in industrial applications. In this work, the effects of exposure time to air, immersion time in the 3.5 wt % NaCl solution, and immersion time in the acid (pH=1) and alkali (pH=12) solutions on the wettability of the superhydrophobic surface were examined. Fig. 11a shows variations of the contact angles and the sliding angles of the superhydrophobic surface as a function of the exposure time to air. Both contact angles and

sliding angles are slightly changed during air exposure for 8 weeks, which indicates that the superhydrophobic surface has good long-term stability in air. The changes of the contact angles and sliding angles with increasing immersion time in the 3.5 wt % NaCl solution are shown in Fig. 11b. The contact angles gradually decrease and the sliding angles gradually increase with the increase of immersion time. A contact angle of 153° and the a sliding angle of 6^{o} are still maintained after immersing in the solution for 24 h, indicating that the long-time immersion in the 3.5 wt % NaCl solution don't have great influence on the superhydrophobicity of the as-prepared surface. Fig. 11c displays the variation of the contact angles with immersion time in acid (pH=1) and alkali (pH=12) solutions. The pH value was adjusted by hydrochloric acid and sodium hydroxide. In the case of the alkali solution, the contact angle decreases to 148° after immersion only for 20 min. This result derives from the strong reaction between the superhydrophobic Al alloy surface and the strong alkali solution, because the produced gas is observed near the superhydrophobic surface during the immersion process. In contrast, the as-prepared surface retains superhydrophobicity after immersion in the acid solution for 12 h, which suggests that the as-prepared superhydrophobic surface has good chemical stability in acidic environment. In conclusion, the as-prepared superhydrophobic Al alloy surface has long-term stability in air and 3.5 wt % NaCl solution. It also displays good chemical stability in acidic environment but cannot be applied in alkaline environment.

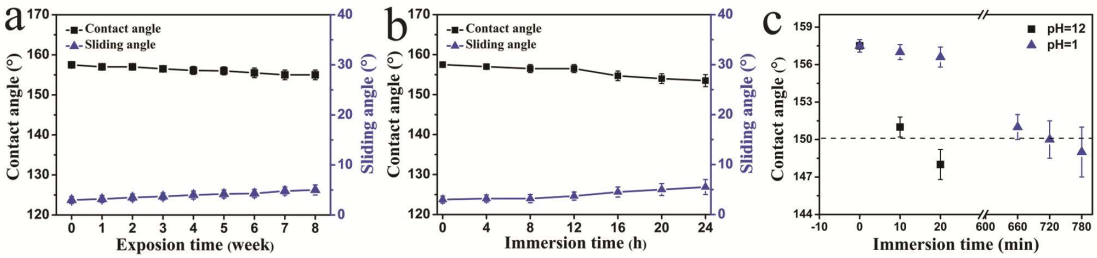

Fig. 11 Variations of the contact angles and sliding angles of the superhydrophobic surface as functions of the exposure time to air (a); immersing time in 3.5 wt.% NaCl solution (b) ; and immersion time in acid (pH=1) and alkali (pH=12) solutions (c)

4 Conclusions

A superhydrophobic Al alloy surface with a contact of 157±0.5° and a sliding angle of 3± 0.7° is successfully fabricated by a facile anodic oxidation and self-assembly process. In addition, the transformation from superhydrophilicity to superhydrophobicity can be achieved by adjusting the modification process for the constructed surface. The superhydrophobicity of the resulting surface derives from its rough surface with hierarchical micro-nanostructures and the assembly of low-surface-energy film on it. The as-prepared superhydrophobic surface has excellent mechanical abrasion resistance, excellent corrosion resistance, and self-cleaning ability as well as long-term stability. The facile and low-cost fabrication process offer an effective strategy and promising industrial applications for fabricating robust, stable and anticorrosion superhydrophobic Al alloy surface.

Supporting information

Videos as described in the captions of Fig. 9 and Fig. 10 can be found in the online version.

Acknowledgments

The authors are grateful to the support of the National Natural Science Foundation of China (Grants: 51275176, 21473061) and the Fundamental Research Funds for the Central Universities (Grants: 2014ZG0014) for financial support.

References

1. K. Liu and L. Jiang, *Nanoscale*, 2011, 3, 825-838.
2. Y. Tian, B. Su and L. Jiang, *Adv. Mater.,* 2014*,* doi: 10.1002/adma.201400883
3. G. Zhou, J. He, L. Gao, T. Ren and T. Li, *RSC Adv*, 2013, 3, 21789-21796.
4. M. Ruan, W. Li, B. Wang, B. Deng, F. Ma and Z. Yu, *Langmuir*, 2013, 29, 8482-8491.
5. K. Li, H. Li and X. Lai, *RSC Adv, 2014,* doi: 10.1039/c4ra01227e
6. X. Zhang, L. Wang and E. Levänen, *RSC Adv*, 2013, 3, 12003-12020.
7. P. Wang, D. Zhang, R. Qiu and J. Wu, *Corros. Sci.*, 2014, 83, 317-326.
8. S. Yuan, S. Pehkonen, B. Liang, Y. Ting, K. Neoh and E. Kang, *Corros. Sci.*, 2011, 53, 2738-2747.
9. M. Li, J. Xu and Q. Lu, *J. Mater. Chem.*, 2007, 17, 4772-4776.
10. L. Cao, X. Lu, F. Pu, X. Yin, Y. Xia, W. Huang and Z. Li, *Appl. Surf. Sci.*, 2014, 288, 558-563.
11. Y. Ding, Y. Li, L. Yang, Z. Li, W. Xin, X. Liu, L. Pan and J. Zhao, *Appl. Surf. Sci.*, 2013, 266, 395-399.
12. C.-F. Wang, H.-Y. Chen, S.-W. Kuo, Y.-S. Lai and P.-F. Yang, *RSC Adv*, 2013, 3, 9764-9769.
13. J. P. Fernández-Blázquez, D. Fell, E. Bonaccurso and A. d. Campo, *J. Colloid Interface Sci.*, 2011, 357, 234-238.
14. J. Vasiljević, B. Tomšič, I. Jerman, B. Orel, G. Jakša, J. Kovač and B. Simončič, *J. Sol-Gel Sci. Technol.*, 2014, 1-15.
15. T. Ishizaki, J. Hieda, N. Saito, N. Saito and O. Takai, *Electrochim. Acta.*, 2010, 55, 7094-7101.
16. B. Qian and Z. Shen, *Langmuir*, 2005, 21, 9007-9009.
17. V. A. Ganesh, A. S. Nair, H. K. Raut, T. T. Y. Tan, C. He, S. Ramakrishna and J. Xu, *J. Mater. Chem.*, 2012, 22, 18479-18485.
18. M. Qu, B. Zhang, S. Song, L. Chen, J. Zhang and X. Cao, *Adv. Funct. Mater.*, 2007, 17, 593-596.
19. R. B. Pernites, C. M. Santos, M. Maldonado, R. R. Ponnapati, D. F. Rodrigues and R. C. Advincula, *Chem. Mater.*, 2011, 24, 870-880.
20. B. K. Nayak, P. O. Caffrey, C. R. Speck and M. C. Gupta, *Appl. Surf. Sci.*, 2013, 266, 27-32.
21. F. Su, K. Yao, C. Liu and P. Huang, *J. Electrochem. Soc.*, 2013, 160, D593-D599.
22. P. Wang, D. Zhang, R. Qiu, Y. Wan and J. Wu, *Corros. Sci.*, 2014, 80, 366-373.
23. T. Verho, C. Bower, P. Andrew, S. Franssila, O. Ikkala and R. H. Ras, *Adv. Mater.*, 2011, 23, 673-678.
24. X. Zhu, Z. Zhang, X. Men, J. Yang, K. Wang, X. Xu, X. Zhou and Q. Xue, *J. Mater. Chem.*, 2011, 21, 15793-15797.
25. X. Zhu, Z. Zhang, J. Yang, X. Xu, X. Men and X. Zhou, *J. Colloid Interface Sci.*, 2012, 380, 182-186.
26. Z. She, Q. Li, Z. Wang, L. Li, F. Chen and J. Zhou, *Chem. Eng. J.*, 2013, 228, 415-424.

27. F. Su and Y. Kai, *ACS Appl. Mater. Interfaces*, 2014, 6, 8762–8770.
28. R. Palanivel, P. Koshy Mathews, N. Murugan and I. Dinaharan, *Materials & Design*, 2012, 40, 7-16.
29. J. Zhang, Y. Deng, W. Yang, S. Hu and X. Zhang, *Materials & Design*, 2014, 56, 334-344.
30. A. M. Md Jani, D. Losic and N. H. Voelcker, *Prog. Mater Sci.*, 2013, 58, 636-704.
31. M. Abdulstaar, M. Mhaede, L. Wagner and M. Wollmann, *Materials & Design*, 2014, 57, 325-329.
32. T. He, Y. Wang, Y. Zhang, T. Xu and T. Liu, *Corros. Sci.*, 2009, 51, 1757-1761.
33. L. Feng, H. Zhang, Z. Wang and Y. Liu, *Colloid Surf. A: Physicochem. Eng. Asp.*, 2014, 441, 319-325.
34. Q. F. Xu and J. N. Wang, *New J. Chem.*, 2009, 33, 734-738.
35. Y. Kim, S. Lee, H. Cho, B. Park, D. Kim and W. Hwang, *ACS Appl. Mater. Interfaces*, 2012, 4, 5074-5078.
36. H. Y. Erbil and C. E. Cansoy, *Langmuir*, 2009, 25, 14135-14145.
37. Y. Xiu, Y. Liu, D. W. Hess and C. Wong, *Nanotechnology*, 2010, 21, 155705.
38. Z. Chen, Y. Guo and S. Fang, *Surf. Interface Anal.*, 2010, 42, 1-6.
39. J. N. Mateo, S. S. Kulkarni, L. Das, S. Bandyopadhyay, G. C. Tepper, K. J. Wynne and S. Bandyopadhyay, *Nanotechnology*, 2011, 22, 035703.
40. I. A. Larmour, S. E. Bell and G. C. Saunders, *Angew. Chem.*, 2007, 119, 1740-1742.